Graphene screen-printed radio-frequency identification devices on flexible substrates

Kirill Arapov[1]**, Kaarle Jaakkola**[2]**, Vladimir Ermolov**[2]**, Guy Bex**[3]**, Eric Rubingh**[3]**, Samiul Haque**[4]**,
Henrik Sandberg**[2]**, Robert Abbel**[3]**, Gijsbertus de With**[1]**, and Heiner Friedrich**[*, 1]

[1] Laboratory of Materials and Interface Chemistry, Department of Chemical Engineering and Chemistry,
  Eindhoven University of Technology, De Zaale, 5612AJ Eindhoven, The Netherlands
[2] VTT Technical Research Centre of Finland, Tietotie 3, 02044 Espoo, Finland
[3] Holst Centre – TNO, High Tech Campus 31, 5656AE, Eindhoven, The Netherlands
[4] Nokia R&D, UK, 21 JJ Thomson Avenue, Madingley Road, Cambridge, CB3 0FA, United Kingdom

* Corresponding author: e-mail h.friedrich@tue.nl

Despite the great promise of printed flexible electronics from 2D crystals, and especially graphene, few scalable applications have been reported so far that can be termed roll-to-roll compatible. Here we combine screen printed graphene with photonic annealing to realize radio-frequency identification devices with a reading range of up to 4 meters. Most notably our approach leads to fatigue resistant devices showing less than 1% deterioration of electrical properties after 1000 bending cycles. The bending fatigue resistance demonstrated on a variety of technologically relevant plastic and paper substrates renders the material highly suitable for various printable wearable devices, where repeatable dynamic bending stress is expected during usage. All applied printing and postprocessing methods are compatible with roll-to-roll manufacturing and temperature sensitive flexible substrates providing a platform for the scalable manufacturing of mechanically stable and environmentally friendly graphene printed electronics.

Flexible graphene RFID

1 Introduction Solution-processed conductors are key components in many large-scale applications ranging from radio frequency identification (RFID) tags [1–5] and printed solar cells [6–8] to wearable electronics [9] that are typically realized by printing techniques, using metal-based inks. With all the benefits of printing techniques such as relative simplicity, high production capabilities including roll-to-roll (R2R) realization, compatibility with commonly used substrates such as polyethylene terephthalate (PET), polyethylene naphthalate (PEN) and paper, the use of metal-based inks has a few downsides. For instance, the use of inexpensive Cu-based inks is limited due to the ease of oxidation leading to the deterioration of conductive properties, whereas Ag-based inks, depending on the market price of the metal, are relatively expensive.

Phys. Status Solidi RRL **10**, No. 11 (2016)

813

Graphene-based inks, as an alternative to metal-based inks, have several advantages such as low cost, chemical stability and mechanical flexibility, and receive considerable interest from science [10–18] and technology [19]. However, the conductivity of printed graphene is still far lower than that of printed Cu or Ag significantly decreasing the application potential. There are several methods to enhance conductivity of graphene structures, including both long-time thermal annealing [13, 14, 18] and fast photonic annealing [20] reported for binder-based graphene inks, compression rolling [4, 17, 21, 22] reported for binder-free inks, and a combination of photonic annealing and compression rolling reported earlier by us [23]. The latter approach is aiming at maximal reduction of sheet resistance for graphene structures, even for graphene inks with binders and rheology modifiers balancing high conductivity with excellent rheology and high printing definition of ink [24]. Photonic annealing is a fast, contactless method for short-time selective heating of materials with strong optical absorption, such as our printed graphene structures. High density light pulses of a few milliseconds duration selectively heat up the graphene reaching temperatures of more than 500 °C [23]. Therefore, photonic annealing is safe to apply to non- or limitedly-absorbing (in the optical range) PET and paper substrates, avoiding their degradation as is observed in conventional high temperature thermal annealing. Applying this approach we were able to achieve 1.4 $\Omega/\square$ (normalized to a 25 μm thick layer [23]) for a binder-based graphene ink. However, this value is still not sufficient to replace metallic parts in applications that were specifically designed for metal-based inks such as bowtie radio-frequency (RF) antennas with sheet resistances of the metallic part of less than 50 m$\Omega/\square$ [3, 25]. Therefore, printed electronics applications, and, in particular, RF antennas aiming at realization using graphene-based inks with corresponding post-processing methods, should be designed with the higher resistance of graphene conductors in mind.

Very recently, several printed graphene RFID tags with a reasonable performance were demonstrated: one is a meandered-line dipole antennae [4] realized by the previously published compression rolling approach [17, 21] and another is a dipole type [5] antennae. Both designs are demonstrated on paper substrates leaving other industrially relevant plastic substrates such as PET, PEN out of the scope. The dipole design has been realized with a commercial ink, the composition of which according to the patent of the manufacturer may contain conductive polymers, and metal particles [19].

In this paper, we present a fabrication and performance investigation of graphene screen-printed radio frequency identification (RFID) devices operating at industrially viable frequency of 867 MHz, realized on various industrially important flexible substrates such as PET, paper and polyimide. We report on the RFID antenna layout specifically designed for graphene inks and on the corresponding post-processing methods. We demonstrate printing of gra-

phene antennas and their post-processing that combines photonic annealing and subsequent compression rolling as a treatment method to significantly decrease the resistance of graphene conductors. We show that an optimized photonic annealing protocol effectively decreases the resistance of printed layers with no detectable damage to the temperature sensitive substrates. Moreover, we demonstrate that our "roll-to-roll compatible" post-treatment method leads to fatigue resistant composite materials showing less than 1% deterioration of electrical properties after 1000 bending cycles. We believe that the combination of printed graphene with post-processing methods such as photonic annealing followed by compression rolling, along with a congruent design will extend the application range for graphene printed flexible electronics.

2 Experimental details

2.1 Graphene ink preparation For the ink preparation, we used our earlier described method proceeding via gelation and *in situ* solvent exchange [24]. In a typical experiment 100 ml of graphene dispersion with graphene-to-binder ratio 1:2 were transferred into 250 ml round-bottom flask followed by addition of 25 ml of methyl ether of dipropylene glycol (Dowanol DPM, Sigma Aldrich, USA). The dispersion was then evaporated at 73 °C and 400 mbar until no distillate was pouring into the receiver flask. The residue, a thick homogeneous paste was transferred to a container by a spatula and used without any further treatment.

2.2 Screen printing of graphene paste Screen printing was performed using a DEK Horizon 03i (DEK International, UK) semiautomatic screen printer with a 45° angle polyurethane squeegee, at a printing speed of 50 mm s^{-1}. As printing substrates special application paper LumiForte (Stora Enso, Finland), PET foil (Agfa, Belgium) and polyimide foil (Kapton HN, DuPont, USA) were employed.

2.3 Photonic annealing The photonic annealing experiments were performed using a PulseForge 1300 (NovaCentrix, USA) apparatus with a xenon stroboscope lamp combined with a curved mirror, as shown in Fig. 1d. We used the following photonic annealing sequence: 5 consecutive modulated light pulses, where each pulse consists of 5 micropulses (Fig. 2b and c) fired at 370 V, and where the first micropulse lasts for 1 ms and the next four micropulses last 0.1 ms. The time gap between each micropulse is 0.5 ms. The average energy density for a single modulated pulse is 2.33 J cm^{-2}, as measured by a built-in bolometer.

2.4 Thermal annealing Thermal annealing of graphene films on PI substrates was performed using a Heraeus M110 muffle furnace (Thermo Scientific, USA) at 350 °C for 30 min in air.

2.5 Compression rolling Compression rolling was performed using a Goldsmith BK-0090 stainless steel 57 mm roll (Goldsmith, China) using a force of 55–65 N mm^{-2} and a speed of 10 mm s^{-1}. The sample was sandwiched between two 5 mm thick polycarbonate foils to prevent contact between the graphene printed layer and the rolls.

2.6 RFID performance measurements The graphene RFID transponder prototypes were measured using a Tagformance UHF RFID measurement system (Voyantic Ltd., Finland). The measurement is based on defining the transponder activation RF power threshold as a function of frequency in a known and calibrated environment. The transponder prototype in the anechoic measurement chamber is shown in Fig. 4c. In order to keep the flexible transponders in vertical position during the measurement, they were mounted on a styrofoam holder with relative permittivity equal to approximately 1, thus, minimizing its impact on the antenna response.

3 Result and discussion The RFID antennae design was based on the microchip NXP Ucode G2XM (NXP Semiconductors, The Netherlands), which we chose for its ease of integration due to large contact pads. As the microchip completes the transponder assembly its RF impedance needs to match the antennae, i.e., sets the input parameter for the antennae design.

As stated by the manufacturer the RF impedance of the chip is $Z_{IC} = 23 – j209\ \Omega$ at the frequency of 867 MHz. Thus, to match the conjugate impedance, i.e., to ensure that both the microchip and antenna are compatible with each other, the antenna should have the impedance of

$Z_{ant} = 23 + j209\ \Omega$ at the same frequency. This means that the antenna should be sufficiently inductive with a low real impedance part. This was the most difficult challenge for the graphene-based antenna designs as the low conductivity of graphene inks impacts both, radiation efficiency of the antenna and the real part of the antenna impedance.

Taking into account the above considerations, we designed the RFID antennas using the electromagnetic simulation software HFSS 15 (Ansys Inc. USA). The antennae design was optimized in simulations to match the input impedance to the one set by the microchip and to maximize the radiation efficiency. The sheet resistance (R_s) used in the simulation was chosen to be 5 $\Omega/\square$. Lower values of R_s would result in a higher device performance and do not affect the antenna layout (see Supporting Information (SI) for simulation details).

The simulated dipole antenna design is shown in Fig. 1a. The size of the opening in the center of the antenna determines the reactance of its impedance as the length and the width of the antenna affect mostly the real part of the impedance. Unlike the commercial transponders made with metal-based inks, the proposed antenna has a simple wide and long conductor shape without meanders that would increase conductivity losses. Figure 1a also shows the final transponder assembly with the microchip displayed in red. Considering fabrication tolerances, inaccuracy of the model and possible variations of the antenna conductivity, a number of prototypes was designed with a sweep of parameters. As the tuning of the transponder is most sensitive to the reactance of the input impedance of the antenna, the dimensional parameter affecting the reactance, i.e., the opening sizes a and b were varied (Fig. 1a). Thus, prototype versions and their dimensions are presented in Table S1 (see Supporting Information, Table S2 for the antenna performance simulation results).

Based on the antenna design, a printing screen with a mesh of 165 stainless steel wires per inch and a wire thickness of 50 μm was manufactured (Fig. 1b). These characteristics of the mesh along with the use of a 45 μm thick emulsion layer allow the deposition of printing layers with a dry thickness of more than 15 μm in a single pass using our inks. To print radio-frequency antennas we used an earlier described graphene paste [24] with a reduced graphene-to-binder ratio of 1 : 2. Such a modification did not significantly impact the ink printability (Fig. 1c), however, it resulted in a lower initial resistance. This graphene paste formulation is specifically aimed at maximal reduction of the sheet resistance on account of binder degradation by either prolonged thermal annealing or fast photonic annealing, with subsequent structure restoration by compression rolling, as illustrated in Fig. 1d.

As printing substrates we employed PET foil and LumiForte paper, which are commonly used in printed electronics. Also, as they have negligible light absorption they are often combined with photonic annealing, e.g., for metal-based inks. To compare the efficiency of photonic annealing with long-time thermal annealing, we also used
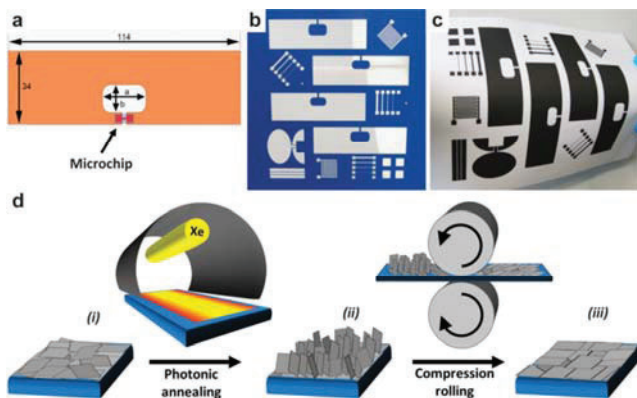

Figure 1 Modelling, screen printing and post-processing of graphene radio-frequency antennas. (a) Radio-frequency identification (RFID) device assembly with antenna (orange) and microchip (red), dimensions are given in mm; (b) photograph of the screen (emulsion side) for printing of graphene antennas, pattern dimensions 180×200 mm^2; (c) graphene antennas screen printed on Lumi paper; (d) scheme of screen printed graphene post-processing, where (i) screen printed sample, (ii) photonically annealed sample, (iii) photonically annealed and compression-rolled sample.

Phys. Status Solidi RRL **10**, No. 11 (2016)

815

Rapid
Research Letter

Table 1 Thermal (350 °C), photonic annealing (PA) and subsequent compression rolling (CR) of printed graphene RFID antennas on flexible.

properties	PI	Lumi paper	PET
thickness, dry, μm	37 ± 3	68 ± 7	45 ± 5
thickness, 350 °C, μm	27		
thickness, PA, μm		80–95	65–75
thickness, CR, μm	10 ± 2	17 ± 2	14 ± 3
R_s, dry, Ω/□	50	31	46
R_s, CR, Ω/□	5.2–3.9	5.0–4.1	7–6
R_s, CR, Ω/□, @ 25 μm	2.1–1.6	2–1.6	5.8–5.0
reading distance before bending, m	3.9	3.1	2.6
reading distance after bending, m	4.0	3.1	2.6

polyimide substrates (PI) that are thermally stable up to 400 °C. To achieve the lowest sheet resistance before post-processing procedures, we increased the thickness of prints by consecutive double layer printing. Thus, on polyimide (PI) substrate we reached 37 μm dry thickness for double prints, whereas, for paper and PET we reached 68 μm and 45 μm dry thickness, respectively (Table 1, see Table S3 for single prints description). Remarkably, printing on paper resulted in the largest layer thickness for all tested substrates. This is most likely due to the capillary force of paper that pulls the graphene paste out of the screen open area upon contact, thus, increasing the deposited ink volume.

As a first step of post-processing, the printed and dried at 100 °C graphene antennas were subjected to thermal treatment by means of either prolonged thermal annealing, i.e., 350 °C for 30 min in air for PI foils or fast photonic annealing for temperature sensitive substrates (Fig. 1d). Having a sample placed on Al-holder (heat sink, Fig. 2a) we employ an optimized sequence comprising 5 consecutive modulated light pulses (Fig. 2b) to be able to quickly reach and maintain high temperature for the duration of irradiation. Each modulated pulse consist of 5 micropulses (Fig. 2c) fired at 370 V, where the first micropulse lasts for 1 ms and the next four micropulses last 0.1 ms. The time gap between each micropulse is 0.5 ms. The average energy density for a modulated pulse is 2.33 J cm^{-2} measured by a built-in bolometer. Temperature measurement of graphene antennas on the chosen substrates during photonic annealing is difficult, thus, to have an idea on temperature distribution within the sample, we performed modelling of the photonic annealing using SimPulse software (Nova-Centrix Inc, USA, see Supporting Information). The results shown in Fig. 2b reveal that the graphene layer reaches high temperature and maintains it for the duration of the modulated pulse, i.e., 3.9 ms (Fig. 2c), followed by a steep decrease. However, heating up of the substrate, which is due to local thermal conduction from the graphene layer, occurs with a delay reaching significantly lower values
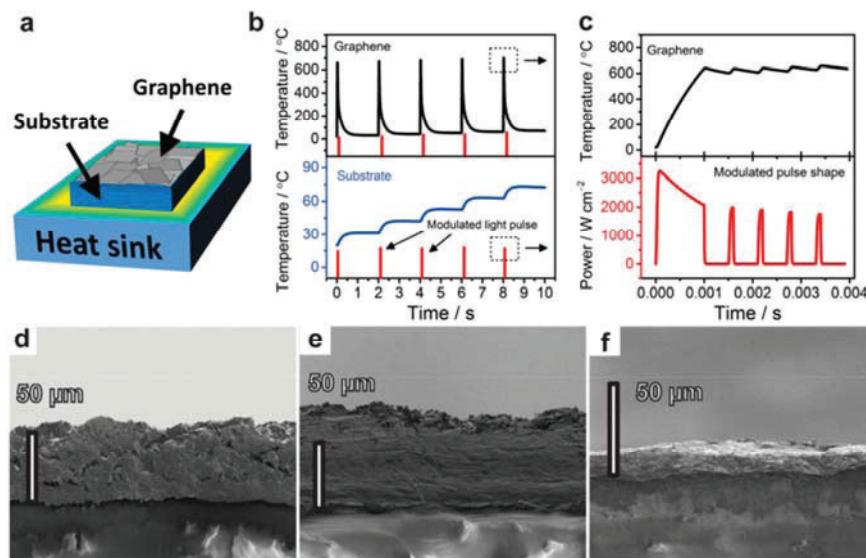

Figure 2 Photonic annealing and compression rolling. (a) Simulation scheme for photonic annealing of printed graphene on temperature sensitive substrate placed on Al-sample holder acting as a heat sink; (b) simulated temperature profiles for 25 μm thick graphene (upper graph, black) layer on 125 μm thick paper substrate (lower graph, blue) with aluminium sample holder underneath acting as a heat sink. Red lines correspond to modulated light pulses with an average output energy 2.3 J cm^{-2} fired at 0.5 Hz (For simulation details see Supporting Information.) Selected areas (dashed squares) correspond to graphs described in Fig. 2b; (c) temperature profile of the graphene layer corresponding to a single modulated light pulse (upper graph, black). Shape of a single modulated light pulse comprising 5 consecutive micropulses: 1 pulse at 370 V, 1 ms + 4 pulses at 370 V, 0.1 ms. The time gap between each micropulse is 0.5 ms while the total modulated pulse time is 3.9 ms (lower graph, red). Cross-sectional SEM micrograph of (d) printed and dried graphene antenna on PET; (e) dried and photonically annealed graphene antenna on PET; (f) dried, photonically annealed and compression rolled graphene antenna on PET.

(Fig. 2b, lower graph). Besides, the heat is quickly absorbed by an Al-holder resulting in a heat removal maintaining the temperature of less than 100 °C. Thus, due to only local and indirect heating (i.e., by thermal transport and not by photonic annealing) as well as by utilization of a heat sink damage to temperature sensitive substrates (paper, PET) can be minimized.

Photonic annealing resulted in a decrease of sheet resistances of approximately 2.5 times as compared to dried layers. The decrease is less pronounced than we reported earlier for printed graphene inks on glass substrates (5 times, see [21]), which is due to a lower energy input. The higher energy input results in a lower sheet resistance, however, it also deteriorates the plastic or paper substrates that were used here, and, thus, had to be avoided. Prolonged thermal annealing resulted in a decrease of sheet resistance by a factor of 3 and about 30% thickness shrinkage (Table 1).

As reported earlier [23], annealing by light pulses leads to quick vaporization and release of solvent and binder molecules trapped between graphene sheets causing layer expansion. Despite the decrease of sheet resistance, the loss of structural integrity reduces the application potential of photonic annealing for thick graphene printed layers as the only method. However, the subsequent utilization of compression rolling (Fig. 1d) for photonically expanded samples enables the restoration of structural integrity along with further decrease of sheet resistance (Table 1). We followed the changes of printed graphene layer upon drying, photonic annealing and compression rolling by cross-sectional scanning electron microscopy. In comparison with just dried graphene layers (Fig. 2d), the films after photonic annealing show an increase in thickness indicating photonically induced expansion. The application of compression rolling leads to compacted layers (Fig. 2e) along with an additional decrease of sheet resistances (Table 1). Contrary to photonic annealing, thermal annealing does not result in layer expansion (Fig. S3, Supporting Information) due to a much slower heat transfer. The compression rolling of thermally annealed layers leads to comparable films (Fig. 2f) with a similar compacted structure (Fig. S3c, SI) with even lower sheet resistance (Table 1). We attribute this to a more complete binder degradation and desorption of contaminants from the surface of graphene sheets. The application of described here post-processing approach enables realization of RFID antennas on PET (Fig. 3a), polyimide (Fig. 3b), and paper (Fig. 3c) flexible substrates. We analysed the material after each processing step, i.e., printing, photonic annealing and compression rolling, by Raman spectroscopy (Fig. S4, SI) Chemical characterization is done by Raman spectroscopy as the usually applied method XPS has a penetration depth of only 5 nm to 10 nm, its results are sensitive to surface roughness, our films have a thickness of about 50 μm to 70 μm and vary in roughness.

No significant differences between the spectra are observed, indicating that post-processing does not alter the
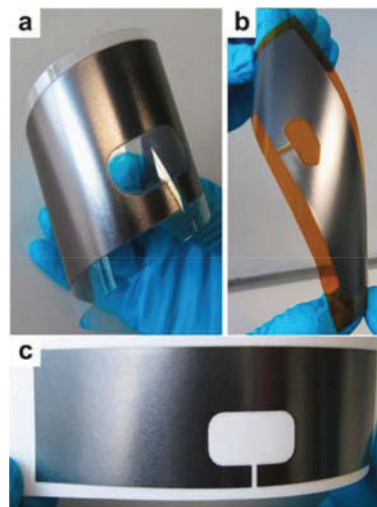

Figure 3 Printed and post-processed graphene RFID antennas on (a) PET, (b) polyimide, and (c) paper substrates.

chemical nature of the layer and maintains a defect density within acceptable levels.

To investigate the structural integrity of annealed and compression rolled graphene films we measured the resistance variations during bending cycling. Thus, strips ($L \times W = 11.3 \times 0.9$ mm^2, Fig. S5, SI) of annealed and compression-rolled graphene films on each substrate were subjected to 1500 bending cycles at 1 Hz using a three point bending system (Fig. 4a) with a bending radius of 5 mm and a span length of 10 mm. During the bending cycles the resistance was measured and variations of less than 0.3% (Fig. 4b) were detected. Overall, less than 1% change in resistance after 1500 cycles was observed. We did not observe any delamination, visible cracks, deformation of the material or substrate, indicating excellent mechanical stability for the current experimental conditions.

The graphene antennas were integrated with the microchips to complete the assembly of the RF identification devices and their performance was analysed using Tagformance (Voyantic Ltd., Finland) UHF RFID measurement system combined with an anechoic chamber (Fig. 4c) [26]. Each graphene device was analysed, and, thereafter, the influence of bending fatigue on performance was investigated, i.e., after the reading range measurements each graphene device has been subjected to 1000 bending cycles with a span of 40 mm and a bending radius of ~42.5 mm per cycle. After these 1000 cycles the performance of graphene transponders was measured again. We did not find any influence of bending on the transponder reading distance demonstrating similar behaviour in a frequency sweep (Fig. 4d, Table 1), indicating excellent fatigue resistance of devices, at least for the described experimental conditions.

We found that the reading distance for graphene devices is different for each substrate reaching 2.6 m for PET foil (Fig. 4e), 3.1 m for paper (Fig. 4f), and 4.0 m for polyimide (Fig. 4g) substrates. As the design of the antennae
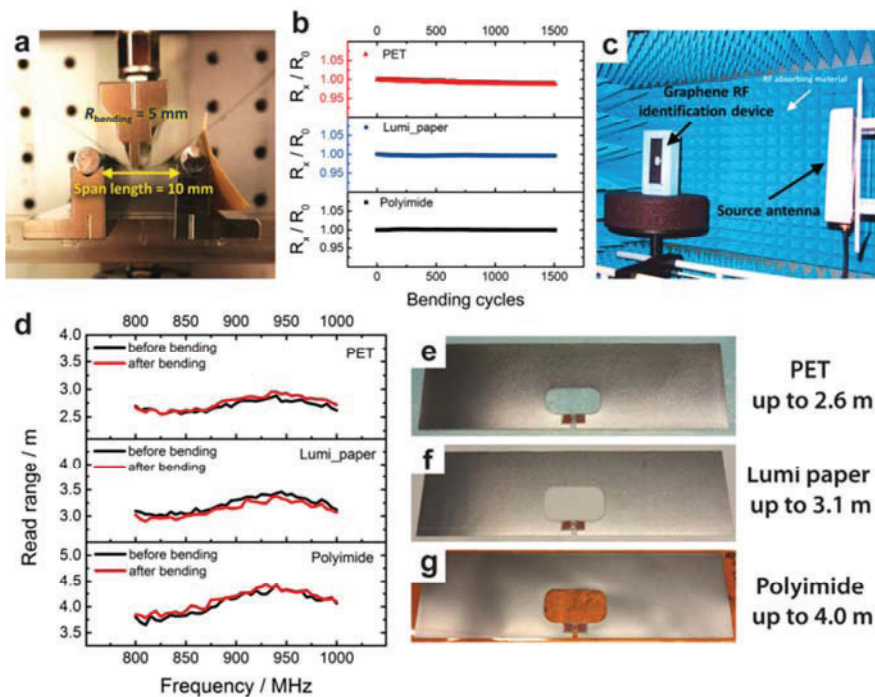
Figure 4 Bending and performance investigation of graphene RF identification devices. (a) Three point bending setup with a bending radius of 5 mm and span length (s) of 10 mm; (b) variation of resistance as a function of bending for 1500 cycles ($R_{bending}$ = 5 mm, s = 10 mm, 1 Hz); (c) measurement of graphene RFID tag in an anechoic chamber; (d) reading range as a function of frequency before and after 1000 bending cycles. Graphene RF identification devices on (e) PET; (f) Lumi paper; (g) polyimide substrates with corresponding reading ranges at the frequency of 867 MHz (on the right).

was optimized for a sheet resistance below 5 $\Omega/\square$, evaluation RFID performance of as printed or photonically annealed structures (which have a higher sheet resistance) is inherently flawed and, hence, omitted. The difference between the simulated (~4.2 m) and measured reading ranges (Table 1) can be considered as an acceptable accuracy at this frequency. Furthermore, variations can be explained by the contact resistance between the graphene films and copper contacts of the microchips as in our simulation model a perfect galvanic contact was assumed. In reality this is not achievable as there are always contaminations present on the materials' surfaces contributing to the resistance. Thus, in the case of thermally annealed samples graphene is considered to be cleaner, demonstrating a lower contact resistance (higher read range), while in the case of photonically annealed samples (PET, paper), the presence of residue binder appears to increase contact resistance, thus, lowering the reading range. In addition, the difference between reading distances for samples on paper and PET can be explained by poorer substrate wetting for the latter, which is supported by thickness difference. Poor wetting can lead to local inhomogeneity of coverage affecting overall conductivity and, thus, reading distance.

The reading range of a transponder is determined by the antenna efficiency, microchip sensitivity and the impedance match between the antenna and the microchip. The microchip NXP Ucode G2XM used in the current studies has a sensitivity of –15 dBm. The NXP chip was specifically chosen as it was available with two large contact pads of copper, which makes bonding with silver paste to the antenna rather easy. For comparison, if more sensitive microchips were used instead, e.g., Impinj Monza R6 with a sensitivity of –20 dBm, the reading distance of gra-

phene transponders would be much larger. For instance, the device on polyimide substrate would have a reading range of 7.3 m, as shown in Table S2, SI.

4 Conclusion In this paper we demonstrated a fabrication and performance investigation of screen-printed graphene RF identification devices on flexible substrates. We showed a dipole RFID antenna layout aiming at maximizing performance for graphene-based devices. Graphene antennas were screen-printed using graphene paste formulated with a graphene-to-binder ratio of 1:2, aiming at minimizing sheet resistance. To decrease the sheet resistance further we utilized a combination of thermal treatment (photonic annealing or long-time thermal treatment) and subsequent compression rolling, reaching sheet resistances of 5 $\Omega/\square$ and lower. We demonstrated the photonic annealing protocol optimized for temperature sensitive substrates (PET and paper) comprising the use of modulated light pulses to quickly reach and maintain high temperature for the duration of pulses, at the same time not damaging the substrates. We found that graphene antennas manufactured using our approach show no degradation of conductivity (<0.3% variation, <1% long-term change) after 1500 bending cycles and, thus, are mechanically stable. The reading range of the graphene devices spans up to 4 meters depending on the sheet resistance of graphene antennas and does not deteriorate after 1000 bending cycles. Such an excellent fatigue resistance opens up many possibilities for the application of our materials and approach for the realization of various printable wearable devices, where repeatable dynamic bending stress levels are expected during usage. The approach demonstrated here encompasses an industrially relevant printing technique, post-

processing methods compatible with roll-to-roll manufacturing paradigms and temperature sensitive flexible substrates. This results in a highly conductive, mechanically stable and environmentally friendly materials providing a platform for manufacturing of graphene printed electronics.

Supporting Information Additional supporting information may be found in the online version of this article at the publisher's website.

References

[1] G. A. Casula, G. Montisci, and G. Mazzarella, IEEE Antennas Wireless Propag. Lett. **12**, 1400 (2013).

[2] J. Perelaer, B. J. de Gans, and U. S. Schubert, Adv. Mater. **18**, 2101–2104 (2006).

[3] A. Rida, Y. Li, R. Vyas, and M. M. Tentzeris, IEEE Antennas Propag. Mag. **51**, 13 (2009).

[4] T. Leng, X. Huang, K. Chang, J. Chen, M. A. Abdalla, and Z. Hu, IEEE Antennas Wireless Propag. Lett. **15**, 1565 (2016).

[5] M. Akbari, M. W. A. Khan, M. Hasani, T. Bjorninen, L. Sydanheimo, and L. Ukkonen, IEEE Antennas Wireless Propag. Lett. **15**, 1569 (2016).

[6] J. S. Yu, I. Kim, J. S. Kim, J. Jo, T. T. Larsen-Olsen, R. R. Sondergaard et al., Nanoscale **4**, 6032 (2012).

[7] D. Kaduwal, H.-F. Schleiermacher, J. Schulz-Gericke, T. Kroyer, B. Zimmermann, and U. Würfel, Sol. Energy Mater. Sol. Cells **124**, 92 (2014).

[8] D. Angmo, T. T Larsen-Olsen, M. Jørgensen, R. R. Søndergaard, and F. C. Krebs, Adv. Energy Mater. **3**, 172 (2013).

[9] M. Stoppa and A. Chiolerio, Sensors **14**, 11957 (2014).

[10] K. Arapov, R. Abbel, G. de With, and H. Friedrich, Faraday Discuss. **173**, 323 (2014).

[11] D. J. Finn, M. Lotya, G. Cunningham, R. J. Smith, D. McCloskey, J. F. Donegan et al., J. Mater. Chem. C **2**, 925 (2014).

[12] J. Li, F. Ye, S. Vaziri, M. Muhammed, M. C. Lemme, and M. Ostling, Adv. Mater. **25**, 3985 (2013).

[13] E. B. Secor, S. Lim, H. Zhang, C. D. Frisbie, L. F. Francis, and M. C. Hersam, Adv. Mater. **26**, 4533 (2014).

[14] E. B. Secor, P. L. Prabhumirashi, K. Puntambekar, M. L. Geier, and M. C. Hersam, J. Phys. Chem. Lett. **4**, 1347 (2013).

[15] K. Y. Shin, J. Y. Hong, and J. Jang, Adv. Mater. **23**, 2113 (2011).

[16] F. Torrisi, T. Hasan, W. Wu, Z. Sun, A. Lombardo, T. S. Kulmala et al., ACS Nano **6**, 2992 (2012).

[17] X. Huang, T. Leng, X. Zhang, J. C. Chen, K. H. Chang, A. K. Geim et al., Appl. Phys. Lett. **106**, 203105 (2015).

[18] W. J. Hyun, E. B. Secor, M. C. Hersam, C. D. Frisbie, and L. F. Francis, Adv. Mater. **27**, 109 (2015).

[19] J. M. Crain, J. S. Lettow, I. A. Aksay, S. A. Korkut, K. S. Chiang, C.-H. Chen, and R. K. Prud'homme, Printed Electronics. USA: Vorbeck Materials Corporation, 2012.

[20] E. B. Secor, B. Y. Ahn, T. Z. Gao, J. A. Lewis, and M. C. Hersam, Adv. Mater. **27**, 6683 (2015).

[21] H. Malekpour, K. H. Chang, J. C. Chen, C. Y. Lu, D. L. Nika, K. S. Novoselov et al., Nano Lett. **14**, 5155 (2014).

[22] X. Huang, T. Leng, M. Zhu, X. Zhang, J. Chen, K. Chang et al., Sci. Rep. **5**, 18298 (2015).

[23] K. Arapov, G. Bex, R. Hendriks, E. Rubingh, R. Abbel, G. de With et al., Adv. Eng. Mater., DOI 10.1002/adem.201500646 (2016).

[24] K. Arapov, E. Rubingh, R. Abbel, J. Laven, G. de With, and H. Friedrich, Adv. Funct. Mater. **26**, 586–593 (2016).

[25] Y. Amin, Q. Chen, L.-R. Zheng, and H. Tenhunen, Prog. Electromagn. Res. **130**, 1–15 (2012).

[26] K. V. S. Rao, P. V. Nikitin, and S. F. Lam, IEEE Trans. Antennas Propag. **53**, 3870 (2005).